Microwave/millimeter wave sensors

Towards Localization of Miniaturized Medical Robots With Microwaves

Yu-Hsiang Lin[1], Hugo Daguerre[1], Anastasia Lavrenko[2*], and Sarthak Misra[1,3**]

[1] *Surgical Robotics Laboratory, Department of Biomechanical Engineering, University of Twente, 7522LW Enschede, The Netherlands*
[2] *Radio Systems Group, Faculty of Electrical Engineering, Mathematics and Computer Science, University of Twente, 7522NH Enschede, The Netherlands*
[3] *Surgical Robotics Laboratory, Department of Biomaterials and Biomedical Technology, University of Groningen and University Medical Centre Groningen, 9713GZ Groningen, The Netherlands*
[*] *Member, IEEE*
[**] *Senior Member, IEEE*

Manuscript received 22 March 2024; revised 18 May 2024; accepted 6 June 2024. Date of publication 11 June 2024; date of current version 4 July 2024.

Abstract—The emergence of miniaturized medical robots capable of performing targeted therapeutic procedures in deep-seated anatomical regions presents an alternative to conventional medical treatments. However, it remains a significant challenge to accurately locate the miniaturized robots in the complex environments of living organisms. Taking advantage of the short wavelength and noninvasive nature, microwave sensing holds promise in detecting small foreign objects embedded in tissue based on their dielectric properties. However, the limiting factor is the tradeoff between the penetration depth and the wavelength of the microwave signals. In this letter, we investigate the feasibility of using microwave signals in the frequency range from 18 to 40 GHz to detect centimeter to millimeter-scale metallic objects behind tissue-mimicking gelatin screens. The insights obtained from this work pave the way for the development of novel strategies for the localization of miniaturized medical robots using microwaves.

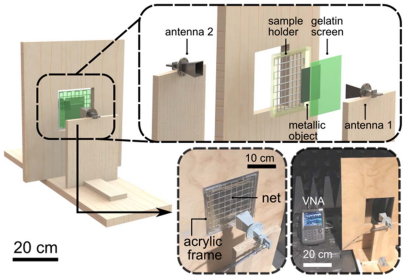

Index Terms—Microwave/millimeter wave sensors, miniaturized medical robots (MMRs), object detection.

I. INTRODUCTION

Over the years, a variety of different components have been developed that are essential for the autonomous control of miniaturized medical robots (MMRs), including actuators [1], [2], [3], [4], sensors [5], [6], and localization systems [7], [8]. Accurate localization of the MMRs in the human body is crucial for enabling precise control and navigation. However, this task is challenging due to the typically small dimensions of the MMRs, which range from a few centimeters to a sub-millimeter scale. Conventional medical imaging techniques, such as magnetic resonance imaging [9], computed tomography scanning [10], or ultrasound [11], have been investigated as potential means of tracking MMRs. However, these imaging modalities are either not suitable for patients with metallic medical implants, utilize ionizing radiation, or provide limited spatial resolution. In contrast, microwave-based sensing distinguishes objects by their dielectric properties, which could enable the tracking of MMRs with high spatial and temporal resolution [12], [13].

Microwave signals in the sub- to low-gigahertz range have been used successfully in a variety of biomedical applications, including tissue ablation and wireless power transfer for medical implants [14], [15], [16]. Signals in this frequency range are able to reach a deeply situated target in the human body [17]. However, the wavelengths in the centimeter range are generally not suitable for detecting MMRs with dimensions ranging from a few millimeters to micrometers [18]. On the other hand, at millimeter-wave frequencies (upper gigahertz range), the tissue absorption rate increases dramatically, quickly limiting the signal penetration depth [19]. Generally, signals at higher frequencies allow detection of smaller objects, but they get attenuated stronger in the scattering media. Therefore, the feasibility of using microwaves for tracking MMRs depends on striking a balance between the desired spatial resolution and the tissue penetration capabilities. In this work, we investigate the possibility of using electromagnetic signals in the upper microwave range (from 18 to 40 GHz) to detect MMRs. We first characterize the signal attenuation properties of bio-mimicking media, i.e., gelatin screens, and then evaluate how well we can detect metallic objects behind the gelatin screen based on the measured reflection coefficient.

II. EXPERIMENTAL SETUP

We design an experimental setup (see Fig. 1) to measure the attenuation properties of the tissue-mimicking gelatin material (scattering medium) and the reflection characteristics of the metallic objects (target). The setup includes a sample holder that is placed between two broadband horn antennas (LB-180400H-KF, A-info, Inc., USA) connected to a vector network analyzer (VNA) (N9952 A, Keysight Technologies, USA) [see Fig. 1(d)]. The sample holder is made of an acrylic frame with an opening supported by a fabric-based net to keep the gelatin screen in place [see Fig. 1(b) and (c)]. The size of the opening, i.e., $160 \times 160 \times 3$ mm^3, is chosen to ensure that the antenna beams fit fully within it and the sample holder does not affect measurement results, which was confirmed during preliminary setup testing. The measurement setup was calibrated prior to the start of measurements using a standard mechanical calibration kit

Corresponding author: Sarthak Misra (e-mail: s.misra@utwente.nl).
Associate Editor: Giacomo Langfelder.
Digital Object Identifier 10.1109/LSENS.2024.3412400

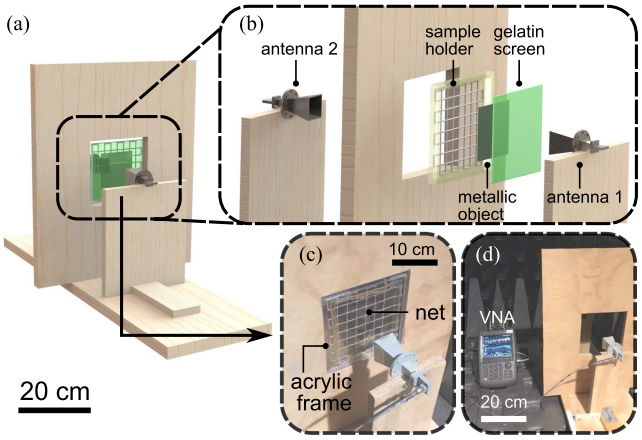

Fig. 1. Experimental setup. (a) Computer-assisted design model with the scale bar (black) depicting 20 cm. (b) Expanded view of the model, including a sample holder, a metallic object, a gelatin screen, a transmitting antenna (antenna 1), and a receiving antenna (antenna 2). (c) Close-up view of the actual sample holder including an acrylic frame and a fabric-based net with the scale bar (black) depicting 10 cm. (d) Broad view of the actual setup, including the VNA with the scale bar (white) depicting 20 cm.

TABLE 1. Nomenclature and Details of Gelatin Screens and Metallic Objects Used in the Experiments

Nomenclatures	Thickness	Dimensions	Description
Gelatin screens:			
G_1	3 mm	160 × 160 mm^2	"old" sample fabricated **more** than 3 hours before experiment
G_2	3 mm	160 × 160 mm^2	"fresh" sample fabricated **less** than 3 hours before experiment
G_3	6 mm	160 × 160 mm^2	G_2 in front of G_1 with regard to antenna 1
Metallic objects:			
M_1	1 mm	150 × 150 mm^2	steel plate
M_2	1 mm	100 × 100 mm^2	steel plate
M_3	1 mm	50 × 50 mm^2	steel plate
M_4	3 mm	7 × 7 mm^2	standard M4 nut (DIN934)

for 10 MHz to 50 GHz (N4693-60001, Agilent Technologies, USA), and all experiments were carried out in an anechoic chamber to avoid spurious clutter reflections.

Gelatin screens are used as scattering media between the transmitting antenna (antenna 1) and the target (metallic object) [see see Fig. 1(b)]. Two gelatin screens are prepared: a sample is fabricated more than 3 h before the experiments (G_1), and another is fabricated less than 3 h before the experiments (G_2) (see Table 1). Note that since the water content in gelatin decreases with time, having two samples of different ages allows evaluating the effect that the water content has on the attenuation properties of gelatin screens. Furthermore, we combine both gelatin screens placing the gelatin screen G_2 in front of G_1 with respect to the incident signal (G_3 in Table 1). For object detection experiments, different metallic objects, including steel plates of various dimensions (M_1– M_3 in Table 1) and a standard M4 nut (M_4 in Table 1), are tested. The dimensions of the gelatin screens and metallic objects used in the experiments are given in Table 1.

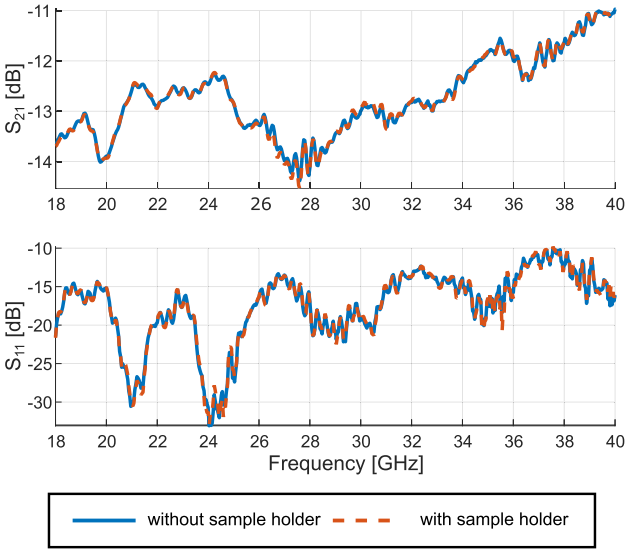

Fig. 2. Reference look-through measurements of the transmission (S_{21}) and reflection (S_{11}) coefficients without gelatin screens.

Using our experimental setup, we investigate signal propagation through gelatin screens in the frequency range from 18 to 40 GHz with a frequency step of 40 MHz. In the following section, measurement results of the reflection coefficient (S_{11}) and the transmission coefficient (S_{21}) are shown. The reflection coefficient (S_{11}) indicates how much signal power is reflected back at the reference plane of antenna 1 when it acts as a transmitting antenna, while the transmission coefficient (S_{21}) shows how much power is received by antenna 2 when it acts as a receiving antenna. Note that since our setup is not a closed system, power loss occurs during wave propagation. Nonetheless, measuring scattering parameters enables indirect evaluation of the attenuation properties of gelatin screens by comparing the results with reference measurements.

III. RESULTS AND DISCUSSION

A. Look-Through Experiment

The attenuation properties of the gelatin screens are evaluated by measuring the scattering parameters in the look-through experiments. Note that all presented curves represent an average over the results of three independent measurements. As a reference, we first measure S_{11} and S_{21} without the gelatin screens. The results are presented in Fig. 2 for two cases: when only a wooden platform is present without the sample holder, and when the sample holder is added. Since the two measurements are nearly identical, we conclude that the addition of the sample holder, including an acrylic frame and a fabric-based net, does not introduce any unwanted artifacts to the experimental results.

Next, we repeat the measurements with different gelatin screens (G_1–G_3 as defined in Table 1). The results are plotted in Fig. 3. For G_1 and G_2, which have the same thickness but different water content, we observe a linear decrease in S_{21} as the frequency increases. On average, there is a 14 dB loss in signal strength from 18 to 40 GHz. It can also be seen that S_{21} for the gelatin screen G_1 is at least 5 dB higher than for G_2. Furthermore, when the two gelatin screens are placed together (G_3), S_{21} is reduced to the noise level. This observation suggests that with the output power provided by the VNA (which was 0 dBm in our case), microwave signals of the selected range (18–40 GHz) cannot penetrate gelatin with a thickness of 6 mm.

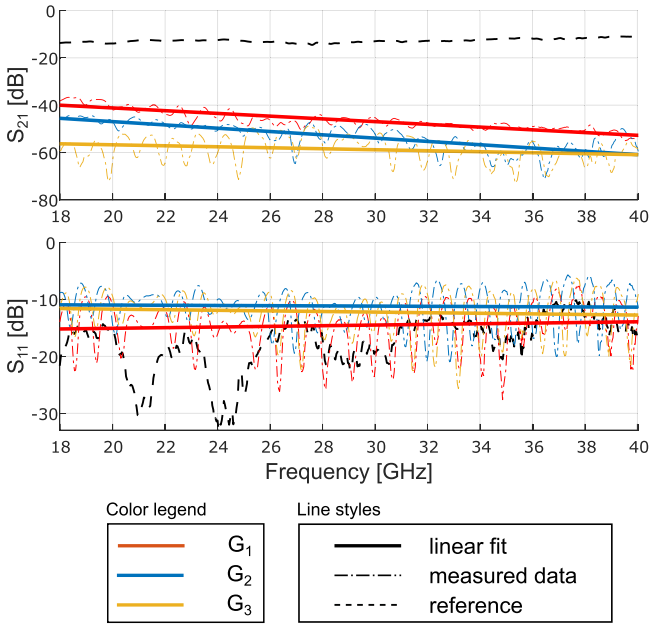

Fig. 3. Look-through measurements of the transmission (S_{21}) and reflection (S_{11}) coefficients with the gelatin screens (G_1–G_3) listed in Table 1, including the reference measurement with no gelatin screen (dashed line), measured data (dash-dotted lines), and linear fit curves (solid lines).

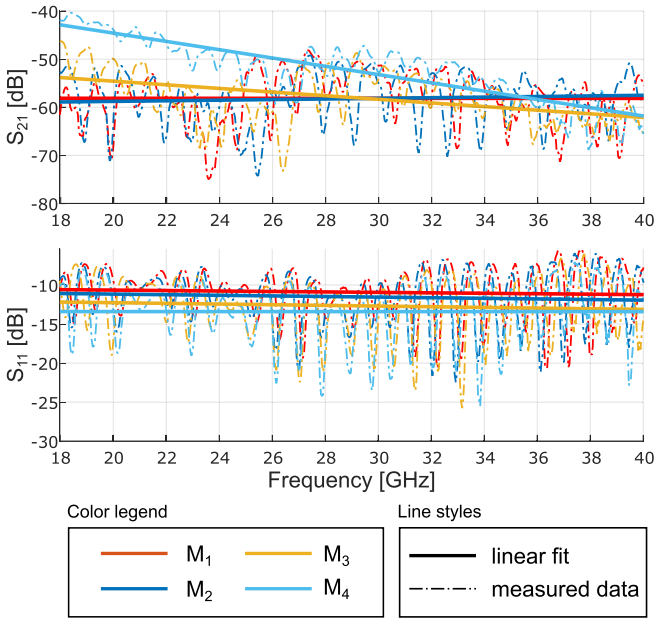

Fig. 4. Object detection measurements of the transmission (S_{21}) and reflection (S_{11}) coefficients in which metallic objects (M_1–M_4) from Table 1 are placed behind the gelatin screen G_2, including measured data (dash-dotted lines) and linear fit curves (solid lines).

TABLE 2. Attenuation Loss of Gelatin Screens At Specific Frequencies

	Attenuation loss (L_{att}) [dB]					
Gelatin screens	18 GHz	20 GHz	26 GHz	30 GHz	36 GHz	40 GHz
G_1	29.3	30.7	34.9	37.7	41.9	44.7
G_2	26.8	27.9	31.4	33.7	37.2	39.5

For the reflection coefficient, we observe that S_{11} values are frequency independent and are largely determined by the properties of the first material that the electromagnetic wave encounters. More specifically, the results for G_2 and G_3 display similar trends and are close in value since both of them have the same gelatin screen (G_2) placed toward antenna 1. On the other hand, S_{11} is 5 dB lower for G_1, indicating that tissues with higher water content reflect a larger portion of the incident wave in this frequency range. Combining this with the results for S_{21} measurements, it also suggests that the difference in water content between the two gelatin screens contributes only marginally to the signal attenuation rate. Note that the difference between the reference S_{21} measurements and the measurements with gelatin screens quantifies the total loss in received signal strength due to the addition of the gelatin screen. It combines the effects of the signal attenuation within the gelatin material and the signal reflection at its surface. Therefore, using reference measurements from Fig. 2, we can evaluate the attenuation loss (L_{att}) in the gelatin screen as

$$L_{att} = S_{21}^{ref}[\text{dB}] - S_{21}^{G}[\text{dB}] + S_{11}^{ref}[\text{dB}] - S_{11}^{G}[\text{dB}] \quad (1)$$

where S_{ij}^{G} and S_{ij}^{ref} stand for the (i, j)th scattering parameters with and without the gelatin screen, respectively. Table 2 provides estimates of the attenuation loss (L_{att}) for G_1 and G_2 at selected frequencies. Our results indicate that a fresh 3 mm gelatin screen attenuates the signal in the selected frequency range by at least 26 dB.

B. Object Detection Experiment

After investigating the attenuation properties of the tissue-mimicking gelatin screens, we evaluate the feasibility of detecting metallic objects embedded behind them. A metallic object is fixed between the gelatin screen G_2 and the sample holder so that the gelatin screen serves as a scattering medium between the transmitting antenna and the metallic object [see Fig. 1(b)]. The purpose of this arrangement is to simulate the localization scenario in which an MMR is embedded in biological tissue. Complete details of the metallic objects used in the experiments are provided in Table 1, while the measured transmission (S_{21}) and reflection coefficients (S_{11}) are presented in Fig. 4.

From the measured transmission coefficient of the smaller metallic objects (M_3 and M_4), one can observe a frequency-dependent signal loss due to the attenuation of the gelatin screen. This trend is similar to the look-through measurement results without the metallic object in Fig. 3. With larger metallic objects (M_1 and M_2), the transmission coefficient is reduced to the noise floor. This outcome can be expected since the signal transmission path is fully blocked when the object size is larger than the effective wavefront area of the transmitted signal.

The measurements of the reflection coefficient (S_{11}), on the other hand, provide a small but clear distinction with regard to object sizes. For instance, the average value of S_{11} for metallic object M_1 is -10.93 dB. It drops to -11.53 dB for M_2, -12.68 dB for M_3, and -13.41 dB for M_4. For comparison, we list the values of the reflection coefficient at specific frequencies in Table 3. As a reference, we also provide the results from Fig. 3 for gelatin screens G_1 and G_2 alone, i.e., without the metallic objects. Since the gelatin screen G_2 has aged during the time between the look-through experiments and the object detection experiments, its properties in the object detection experiment became closer to those of G_1. Therefore, we compare the S_{11} measurements with metallic objects to the measurements of the old gelatin screen (G_1). We observe that the reflection coefficient measured with the embedded metallic object (see Table 3) is higher than the measurement of G_1 from Fig. 3, which is around -15 dB. This

TABLE 3. Reflection Coefficient of Gelatin Screens and Metallic Objects Embedded Behind Gelatin Screen G_2 At Specific Frequencies

	Reflection coefficient (S_{11}) [dB]					
Samples	20 GHz	24 GHz	28 GHz	32 GHz	36 GHz	40 GHz
Gelatin screens:						
G_1	−15.08	−14.86	−14.64	−14.42	−14.19	−13.97
G_2	−11.00	−11.08	−11.16	−11.24	−11.32	−11.40
Metallic objects:						
M_1	−10.65	−10.77	−10.88	−10.99	−11.10	−11.22
M_2	−11.16	−11.31	−11.46	−11.61	−11.76	−11.91
M_3	−12.27	−12.43	−12.60	−12.77	−12.94	−13.10
M_4	−13.41	−13.41	−13.41	−13.41	−13.41	−13.41

suggests that we can detect metallic objects behind a gelatin screen by measuring the scattering parameters. Furthermore, it might also be possible to differentiate objects based on their sizes by comparing the measured reflection coefficient. This result demonstrates the potential of using microwave signals of the considered frequency range to detect objects of varying dimensions.

IV. CONCLUSION

This letter explores the feasibility of using signals in the upper microwave range (from 18 to 40 GHz) for detecting metallic objects embedded behind tissue-mimicking gelatin screens. Based on the measurements of the scattering parameters, we assessed the attenuation of the transmitted signal in the test sample and the reflection of the signal from it. More specifically, measurements of the transmission coefficient offer insight into signal attenuation properties through the scattering media (gelatin screens), while measurements of the reflection coefficient show the signal reflection from the embedded metallic objects. Our analysis of the results suggests that it is possible to detect the presence of metallic objects embedded behind a 3 mm gelatin screen with signals in the specified frequency range. However, improving spatial resolution while providing sufficient penetration depth remains a challenge.

Future investigations will explore strategies to mitigate this challenge. For example, a high-gain antenna with a focused narrow beamwidth can be used to increase the penetration depth despite the use of high-frequency signals. The reduced beamwidth of the high-gain antenna can be compensated for by using a scanning mechanism, for example, by attaching the antenna to a robotic arm. Furthermore, the detection of the reflected signal can be facilitated by adding a radio frequency transponder to an MMR. A possible option for such a transponder could be a passive nonlinear tag that is powered by the illuminating signal, such as the one proposed in [20], for example. These strategies can help enable the use of microwave sensing for the localization of embedded MMRs.

ACKNOWLEDGMENT

The authors would like to thank Dr. Z. Mahfouz for helping set up the experiments. This work was supported by the European Research Council (ERC) through the European Union's Horizon 2020 Research and Innovation programme under Grant 866494 project - MAESTRO.

REFERENCES

[1] K. E. Peyer, L. Zhang, and B. J. Nelson, "Bio-inspired magnetic swimming microrobots for biomedical applications," *Nanoscale*, vol. 5, no. 4, pp. 1259–1272, 2013.
[2] S. Mohanty, A. Paul, P. M. Matos, J. Zhang, J. Sikorski, and S. Misra, "CeFlowBot: A biomimetic flow-driven microrobot that navigates under magneto-acoustic fields," *Small*, vol. 18, no. 9, 2022, Art. no. 2105829.
[3] S. Mohanty, Y.-H. Lin, A. Paul, M. R. van den Broek, T. Segers, and S. Misra, "Acoustically actuated flow in microrobots powered by axisymmetric resonant bubbles," *Adv. Intell. Syst.*, vol. 6, no. 1, 2023, Art. no. 2300465.
[4] J. Zhang, X. Zheng, H. Cui, and Z. Silber-Li, "The self-propulsion of the spherical Pt–SiO2 janus micro-motor," *Micromachines*, vol. 8, no. 4, 2017, Art. no. 123.
[5] K. Yoshida and H. Onoe, "Marangoni-propulsion micro-robots integrated with a wireless photonic colloidal crystal hydrogel sensor for exploring the aquatic environment," *Adv. Intell. Syst.*, vol. 4, no. 5, 2022, Art. no. 2100248.
[6] W. Jing and D. Cappelleri, "A magnetic microrobot with in situ force sensing capabilities," *Robotics*, vol. 3, no. 2, pp. 106–119, 2014.
[7] B. Wang, Y. Zhang, and L. Zhang, "Recent progress on micro-and nano-robots: Towards in vivo tracking and localization," *Quantitative Imag. Med. Surg.*, vol. 8, no. 5, pp. 461–479, 2018.
[8] X. Du and J. Yu, "Image-integrated magnetic actuation systems for localization and remote actuation of medical miniature robots: A survey," *IEEE Trans. Robot.*, vol. 39, no. 4, pp. 2549–2568, 2023.
[9] K. Belharet, D. Folio, and A. Ferreira, "Endovascular navigation of a ferromagnetic microrobot using MRI-based predictive control," in *Proc. IEEE/RSJ Int. Conf. Intell. Robots Syst.*, 2010, pp. 2804–2809.
[10] P. B. Nguyen et al., "Real-time microrobot posture recognition via biplane x-ray imaging system for external electromagnetic actuation," *Int. J. Comput. Assist. Radiol. Surg.*, vol. 13, pp. 1843–1852, 2018.
[11] F. Šuligoj, C. M. Heunis, S. Mohanty, and S. Misra, "Intravascular tracking of micro-agents using Medical ultrasound: Towards clinical applications," *IEEE Trans. Biomed. Eng.*, vol. 69, no. 12, pp. 3739–3747, 2022.
[12] R. Chandra, H. Zhou, I. Balasingham, and R. M. Narayanan, "On the opportunities and challenges in microwave medical sensing and imaging," *IEEE Trans. Biomed. Eng.*, vol. 62, no. 7, pp. 1667–1682, 2015.
[13] R. M. Narayanan, "Technical considerations in medical radar," in *Proc. Int. Conf. Body Area Netw.*, 2013, pp. 526–535.
[14] C. L. Brace, "Microwave tissue ablation: Biophysics, technology, and applications," *Crit. Rev. Biomed. Eng.*, vol. 38, no. 1, 2010, Art. no. 13689.
[15] A. Iqbal, P. R. Sura, M. Al-Hasan, I. B. Mabrouk, and T. A. Denidni, "Wireless power transfer system for deep-implanted biomedical devices," *Sci. Rep.*, vol. 12, no. 1, pp. 1–13, 2022.
[16] N. A. Malik, P. Sant, T. Ajmal, and M. Ur-Rehman, "Implantable antennas for biomedical applications," *IEEE J. Electromagn., RF, Microw. Med. Biol.*, vol. 5, no. 1, pp. 84–96, 2021.
[17] A. S. Poon, S. O'Driscoll, and T. H. Meng, "Optimal frequency for wireless power transmission into dispersive tissue," *IEEE Trans. Antennas Propag.*, vol. 58, no. 5, pp. 1739–1750, 2010.
[18] T.-Y. Huang, H. Gu, and B. J. Nelson, "Increasingly intelligent micromachines," *Annu. Rev. Control, Robot., Auton. Syst.*, vol. 5, pp. 279–310, 2022.
[19] A. Prokscha et al., "A look through artificial human tissues at Ka-band and D-band," in *Proc. Int. Workshop Mobile Terahertz Syst.*, 2023, pp. 1–5.
[20] A. Kumar and A. Lavrenko, "Compact folded meander-line harmonic tag antenna for insect tracking," in *Proc. Eur. Conf. Antennas Propag.*, 2023, pp. 1–5.